Some aspects in Kelvin-Helmholtz instability with and without Boussinesq approximation

Ilinca-Laura BURDULEA[1,2], Alina BOGOI*,[1]

*Corresponding author
[1]POLITEHNICA University of Bucharest, Faculty of Aerospace Engineering,
Department of Aerospace Sciences,
Splaiul Independentei 313, 060042, Bucharest, Romania,
alina.bogoi@upb.ro*
[2]Rheinisch-Westfälische Technische Hochschule Aachen, Deutchland,
ilinca.burdulea@stud.aero.upb.ro, ilinca.burdulea@rwth-aachen.de

DOI: 10.13111/2066-8201.2021.13.4.3

Received: 24 September 2021/ Accepted: 05 November 2021/ Published: December 2021

Abstract: *The topic of this paper is the Kelvin-Helmholtz instability, a phenomenon which occurs on the interface of a stratified fluid, in the presence of a parallel shear flow, when there is a velocity and density difference across the interface of two adjacent layers. This paper focuses on a numerical simulation modelled by the Taylor-Goldstein equation, which represents a more realistic case compared to the basic Kelvin-Helmholtz shear flow. The Euler system is solved with new modelled smooth velocity and density profiles at the interface. The flux at cell boundaries is reconstructed by implementing a third order WENO (Weighted Essentially Non-Oscillatory) method. Next, a Riemann solver builds the fluxes at cell interfaces. The use of both Rusanov and HLLC solvers is investigated. Temporal discretization is done by applying the second order TVD (total variation diminishing) Runge-Kutta method on a uniform grid. Numerical simulations are performed comparatively for both Kelvin-Helmholtz and Taylor-Goldstein instabilities, on the same simulation domains. We find that increasing the number of grid points leads to a better accuracy in shear layer vortices visualization. Thus, we can conclude that applying the Taylor-Goldstein equation improves the realism in the general fluid instability modelling.*

Key Words: *WENO, Kelvin-Helmholtz, Taylor-Goldstein, Rusanov, Harten-Lax-van Leer Contact, TVD Runge-Kutta*

1. INTRODUCTION

In many situations, flows are subject to fluid instabilities. These physical phenomena are triggered by infinitesimal disturbances that grow extracting either kinetic or potential energy from the base flow. Thus, the development of instability can eventually cascade into turbulence. An important example for this concept is the Kelvin-Helmholtz instability, which occurs when there is a velocity shear at the interface between two fluid layers that have different densities. Kelvin-Helmholtz mechanism is based on the competition between the stabilizing stratification and destabilizing velocity difference in the fluid layers [1-5].

For a continuously varying distribution of both density and velocity, the dynamics of the Kelvin-Helmholtz instability is described by the Taylor-Goldstein equation [4] and its subsequent conclusions. One of these is the Richardson number criterion, one of the most

important results of the small-scale stability theory. This index represents the lower boundary for the complete stability of the system, expressing the ratio of buoyancy to shear production.

The aim of the present work is a new comparison between a simple Kelvin-Helmholtz case and one modelled by the Taylor-Goldstein equation. The behavior of different Riemann solvers (Rusanov, HLLC) is also investigated [6].

2. KELVIN-HELMHOLTZ INSTABILITY

Let us consider the equations of motion with the Boussinesq approximation (i.e. the effects of the variation of density are retained only in buoyancy terms and not in inertia terms) [2]. Here we adopt a dimensionless form. We decompose the variables in sums of a basic flow plus a wave perturbation: $\boldsymbol{v}(x,z,t) = \bar{\boldsymbol{u}} + \boldsymbol{v}'(x,z,t)$, $\rho = \rho_0 + \rho' p(x,z,t) = p_0 - \rho g z + p'(x,z,t)$ where p_0 , ρ_0 are reference values. The pressure also includes a hydrostatic component. Only small-amplitude perturbations are considered for wave dynamics, so we may linearize the equations for the perturbations. These are:

$$\begin{cases} \dfrac{\partial u'}{\partial x} + \dfrac{\partial w'}{\partial z} = 0 \\ \dfrac{\partial u'}{\partial t} + \bar{u}\dfrac{\partial u'}{\partial x} = -\dfrac{1}{\rho_0}\dfrac{\partial p'}{\partial x} \\ \dfrac{\partial w'}{\partial t} + \bar{u}\dfrac{\partial w'}{\partial x} = -\dfrac{1}{\rho_0}\dfrac{\partial p'}{\partial z} \end{cases} \tag{1}$$

By being linear, these admit solutions in the form of trigonometric functions. Phase propagation is accompanied by an increase in amplitude; thus, we are looking for solutions such as:

$$u'(x,z,t) = U(z)e^{i(kx-wt)} \tag{2}$$

$$w'(x,z,t) = W(z)e^{i(kx-\omega t)} \tag{3}$$

$$p'(x,z,t) = P(z)e^{i(kx-\omega t)} \tag{4}$$

As opposed to the wavenumber, which is a real quantity, the frequency ω may be a complex number. The existence of a positive imaginary part in frequency would lead to the unbounded amplitude growth/ increase and instability.

The general solution consists in a linear combination of exponentials. In each layer, the exponentially growing solution will be rejected, retaining only the component that decays away from the interface.

The kinematic condition for the interface between the two fluid layers is applied, followed by matching the total pressures at the interfaces, yielding [2]:

$$g(\rho_2 - \rho_1)S - \frac{\rho_1 S}{k}(k\bar{u}_1 - \omega)^2 = \frac{\rho_2 S}{k}(k\bar{u}_2 - \omega)^2 \tag{5}$$

Introducing the density difference between the two layers $\rho_2 - \rho_1 = \Delta\rho$, we solve the quadratic equation for frequency:

$$\omega_{1,2} = \left[\frac{2k(\rho_1\bar{u}_1 + \rho_2\bar{u}_2)}{\rho_0} \pm \sqrt{\frac{-4k^2\rho_1\rho_2(\bar{u}_1 - \bar{u}_2)^2}{\rho_0^2} + \frac{4(\rho_1 + \rho_2)kg\Delta\rho}{\rho_0^2}}\right]\frac{\rho_0}{2(\rho_1 + \rho_2)} \tag{6}$$

A negative radical will lead to conjugate solutions, one of which is positive and will generate instability. This happens for:

$$\frac{2g\Delta\rho}{k\rho_0} < (\bar{u}_1 - \bar{u}_2)^2 \tag{7}$$

where ρ_0 is the harmonic mean of the two densities of the layers. Equation (7) is equivalent with:

$$\lambda < \frac{\pi\rho_0\Delta\bar{u}^2}{g\Delta\rho} \tag{8}$$

where $\Delta\bar{u}$ stands for the velocity shear between the layers. In other words, all short waves up to a critical wavelength grow in time and lead to instability [4].

3. TAYLOR-GOLDSTEIN EQUATION

The Boussinesq approximation neglects the density variation effect in the inertial terms but considers it in the buoyancy term. The flow becomes more realistic compared to the previous Kelvin-Helmholtz situation with sharp discontinuity in density and velocity, if both, continuous vertical mean flow shear and continuous stratification profile are considered. Boussinesq approximation is not valid anymore. Thus. we decompose the density and the velocity into a continuous stratification basic quantity and a disturbance: $\rho(x,z,t) = \bar{\rho}(z) + \rho'(x,z,t)$, $\boldsymbol{v}(x,z,t) = U(z)\boldsymbol{i} + \boldsymbol{v}'(x,z,t)$. In dimensionless form, the smooth density and velocity profile yields the compressible continuity equation:

$$\frac{\partial\rho'}{\partial t} + \left(U + u'\right)\frac{\partial\rho'}{\partial x} + w'\frac{\partial\rho'}{\partial z} = 0 \tag{9}$$

and the momentum equations:

$$\begin{cases} \dfrac{\partial u'}{\partial t} + U\dfrac{\partial u'}{\partial x} + w'\dfrac{\partial U}{\partial z} = -\dfrac{1}{\rho_0}\dfrac{\partial p}{\partial x} \\ \dfrac{\partial w'}{\partial t} + U\dfrac{\partial w'}{\partial x} = -\dfrac{1}{\rho_0}\dfrac{\partial p}{\partial z} - \dfrac{\rho g}{\rho_0} \end{cases} \tag{10}$$

where g is the gravitational acceleration. By introducing a two-dimensional stream function:

$$u'(x,z,t) = -\frac{\partial\psi}{\partial z}, w'(x,z,t) = \frac{\partial\psi}{\partial x} \tag{11}$$

the corresponding equation system to (1) becomes:

$$\begin{cases} \dfrac{\partial\rho'}{\partial t} + U\dfrac{\partial\rho'}{\partial x} - \dfrac{\partial\psi}{\partial x}\dfrac{\partial\bar{\rho}}{\partial z} = 0 \\ \dfrac{\partial^2\psi}{\partial t\partial z} + \dfrac{\partial U}{\partial z}\left(-\dfrac{\partial\psi}{\partial x}\right) + U\dfrac{\partial^2\psi}{\partial z\partial x} = -\dfrac{1}{\rho_0}\dfrac{\partial p}{\partial x} \\ -\dfrac{\partial^2\psi}{\partial t\partial x} - U\dfrac{\partial^2\psi}{\partial x^2} = -\dfrac{1}{\rho_0}\dfrac{\partial p}{\partial z} - \dfrac{\rho g}{\rho_0} \end{cases} \tag{12}$$

Equation of continuity is equivalent to:

$$\frac{\hat{\rho}(z)g}{\rho_0} = \frac{-N^2\widehat{\Psi}(z)}{U-a} \tag{13}$$

where $a = \omega/k$ is the complex wave velocity and $N$is the Brunt-Väisälä frequency, a measure of fluid stability to vertical displacements defined by.

$$N^2 = -\frac{g}{\rho_0}\frac{d\rho}{dz} \tag{14}$$

Next, the pressure and density perturbation terms are eliminated. A single equation for the perturbation stream function is derived, being known as the *Taylor-Goldstein equation* [7], [8], which is a second order differential equation:

$$(U-a)\left[\frac{d^2\widehat{\Psi}}{dz^2} - k^2\widehat{\Psi}(z)\right] + \left(\frac{N^2}{U-a} - \frac{d^2U}{dz^2}\right)\widehat{\Psi}(z) = 0 \tag{15}$$

with two boundary conditions:

$$\widehat{\Psi}(0) = 0, \widehat{\Psi}(H) = 0 \tag{16}$$

By introducing a potential function:

$$\phi(z) = \frac{\widehat{\Psi}(z)}{\sqrt{U-a}} \tag{17}$$

one gets:

$$\begin{aligned}\int_0^h (U - a_r - ia_i)\,[k^2|\phi|^2 + |\phi_z|^2]dz + \frac{1}{2}\int_0^h U_{zz}|\phi|^2 dz \\ = \int_0^h \frac{4N^2 - {U_z}^2}{4|U-a|^2}(U - a_r + ia_i)|\phi|^2 dz\end{aligned} \tag{18}$$

Which after multiplication with the complex conjugate ϕ^* and integration over the domain $[\boldsymbol{0}, \boldsymbol{H}]$ becomes:

$$\int_0^h (-ia_i)\,[k^2|\phi|^2 + |\phi_z|^2]dz = \int_0^h \frac{4N^2 - {U_z}^2}{4|U-a|^2}(ia_i)|\phi|^2 dz \tag{19}$$

Extracting the imaginary part of the previous equation yields:

$$a_i \int_0^h \left[k^2|\phi|^2 + |\phi_z|^2 + \frac{4N^2 - {U_z}^2}{4|U-a|^2}|\phi|^2\right]dz = 0 \tag{20}$$

Since the integral is always positive if $4N^2 - {U_z}^2 > 0$, it implies that $a_i = 0$ and the fluid is stable. We get the so-called Richardson number (i.e. $Ri(z)$) criterion[7]:

$$\min_z Ri(z) = \min_z \frac{N^2}{{U_z}^2} > \frac{1}{4}, \forall z \tag{21}$$

which is actually the condition for a linearly stable flow.

Moreover, this criterion confirms the intuitive idea that a strong stratification always has a stabilizing effect on a flow.

The aim of this paper is to show in comparison the pattern of the flow for both Kelvin-Helmholtz instabilities and the impact over the flow. This article presents the numerical evolution for some benchmark cases that do not fulfill the conditions (8) and (21). Therefore, we consider the full Euler system of equations which is solved using two Riemann solvers: Rusanov and HLLC. Fluxes at cell interfaces is reconstructed by implementing a fifth order WENO (Weighted Essentially Non-Oscillatory) method. Then, a temporal discretization is done by applying the second order TVD (total variation diminishing) Runge-Kutta method on a uniform grid.

4. SPATIAL DISCRETIZATION

The flux at cell boundaries is calculated by implementing a WENO (Weighted Essentially Non-Oscillatory) method, followed by a Riemann solver.

Firstly, physical fields are reconstructed by calculating the left and right-side values on the cell boundary. Numerical tests are performed on a fifth order WENO scheme, using two different stencils for each "target" cell [9]:

$$S(i) = \{I_{i-2}, I_{i-1}, I_i, I_{i+1}, I_{i+2}\} \tag{22}$$

Approximations of physical fields are found by calculating the cell average values:

$$\bar{v}_i = \frac{1}{\Delta x_i}\int_{x_{i-\frac{1}{2}}}^{x_{i+\frac{1}{2}}} v(\xi)d\xi \tag{23}$$

Different stencils will lead to different approximations. For each interface of the target-cell, the fifth-order polynomial approximation $\bar{f}_{i\pm\frac{1}{2}} = h_{i\pm\frac{1}{2}} + O(\Delta x^5)$ is built by the convex combination of interpolated values $\hat{f}^k\left(x_{i\pm\frac{1}{2}}\right)$:

$$\bar{f}_{i\pm\frac{1}{2}} = \sum_{k=0}^{2} \omega_k \hat{f}^k\left(x_{i\pm\frac{1}{2}}\right) \tag{24}$$

where the weights are defined as:

$$\omega_k = \frac{\alpha_k}{\sum_{l=0}^{2}\alpha_l}, \alpha_k = \frac{\bar{\omega}_k}{(\beta_k + \varepsilon)^p} \tag{25}$$

The smoothness indicators β_k at the stencil S_k are given by:

$$\beta_k = \sum_{l=1}^{2} \Delta x^{2l-1} \int_{x-\frac{\Delta x}{2}}^{x+\frac{\Delta x}{2}} \left(\frac{d^l}{dx^l}\hat{f}^k(x)\right)^2 dx \tag{26}$$

And explicitly, accordingly to [10]:

$$\begin{cases} \beta_0 = \frac{13}{12}(f_{i-2} - 2f_{i-1} + f_i)^2 + \frac{1}{4}(f_{i-2} - 4f_{i-1} + 3f_i)^2 \\ \beta_0 = \frac{13}{12}(f_{i-1} - 2f_i + f_{i+1})^2 + \frac{1}{4}(f_{i-1} - f_{i+1})^2 \\ \beta_0 = \frac{13}{12}(f_i - 2f_{i+1} + f_{i+2})^2 + \frac{1}{4}(3f_i - 4f_{i+1} + f_{i+2})^2 \end{cases} \tag{27}$$

In this way, discontinuities and sharp gradient regions from the stencil are avoided [11]. The numerical fluxes at cell boundaries are used in updating the cell-integrated values for next time step. This paper focuses on analyzing and comparing performances of different solvers: the Rusanov flux and the HLLC (Harten-Lax-van Leer Contact) flux [6].

5. TEMPORAL DISCRETIZATION

The numerical solution of the scalar conservation law is semi-discretized in the spatial domain using a discrete set of points. By this, the spatial partial derivatives will be replaced with appropriate finite differences in the grid points, leading to a system of ordinary differential equations:

$$\frac{d\boldsymbol{U}}{dt} = L(\boldsymbol{U}(t)) \tag{28}$$

Here the discrete operator L is used to solve each equation in time. Thus, we associate the time dependent vector $\boldsymbol{U}(t)$ with $\boldsymbol{U}_j(t) = \boldsymbol{U}(x_j, t), j = \overline{0, N}$.
In this paper, time discretization is implemented using a second order TVD Runge-Kutta (TVDRK2) [12], [13]:

$$\boldsymbol{U}^{(1)} = \boldsymbol{U}^n + \Delta t L(\boldsymbol{U}^n) \tag{29}$$

$$\boldsymbol{U}^{n+1} = \frac{1}{2}\boldsymbol{U}^n + \frac{1}{2}\boldsymbol{U}^{(1)} + \frac{1}{2}\Delta t L\left(\boldsymbol{U}^{(1)}\right) \tag{30}$$

6. NUMERICAL TESTS

For both cases of velocity and density profiles, the instability was studied on a domain comprised of two layers of fluid, each with its own velocity and density. The grid spacing was constant. For all the numerical tests, the boundary conditions type was periodic. The initial conditions for the two layers were:

- for the upper one:

$$\rho_1 = 1, u_1 = 0.5, v_1 = 0.01\, sin(\, kx), p_1 = 2.5 \tag{31}$$

- for the bottom one:

$$\rho_2 = 2, u_2 = -0.6, v_2 = 0.01\, sin(\, kx), p_2 = 2.5 \tag{32}$$

where $k = 2\pi/L$ and L is the length of the domain (the distance from the western frontier to the eastern frontier, which is equal to the vertical distance between the frontiers as well). The boundary conditions were transmissive. All the parameters listed above are dimensionless, with respect to the dimensionless formulation of Euler system.

For the discontinuous case of Kelvin-Helmholtz instability (Figs. 1-2), the critical wavelength was computed as:

$$\lambda_{cr} = \frac{\pi\rho_0 \Delta\bar{u}^2}{g\Delta\rho} = 5{,}067 \tag{33}$$

which is clearly greater by the wavelength corresponding to the perturbation we introduced in the system $\lambda = 1$. The critical wavelength stability criterion is thus verified.

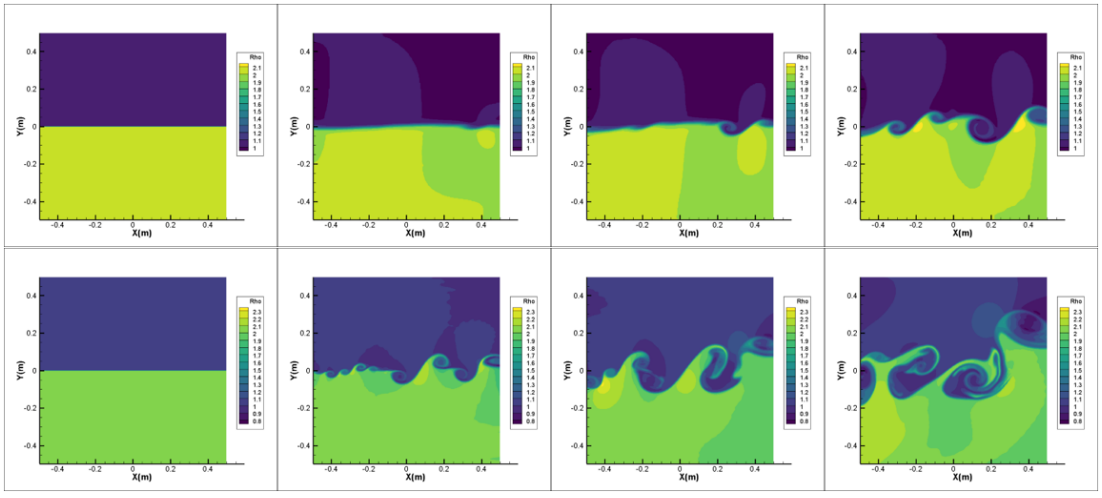

Fig. 1 The evolution of density field for the Kelvin-Helmholtz instability for discontinuous velocity and density profiles. Case: 250×250 grid points, Rusanov (up) versus HLLC (down) solver performance $(t_0 = 0s, t_1 = 0{,}72s, t_1 = 1{,}02s, t_1 = 1{,}38s)$

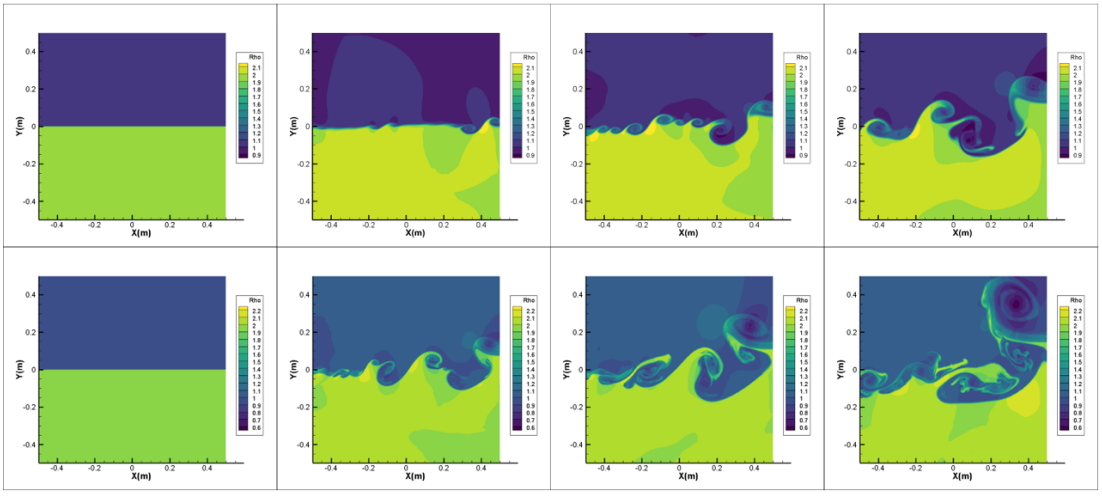

Fig. 2 The evolution of density field for the Kelvin-Helmholtz instability for discontinuous velocity and density profiles. Case: 500×500 grid points, Rusanov (up) versus HLLC (down) solver performance $(t_0 = 0s, t_1 = 0{,}72s, t_1 = 1{,}02s, t_1 = 1{,}38s)$

For the continuous case of the Kelvin-Helmholtz instability (Figs. 3-4), besides the fluid parameters which are the same, the added proposed smooth velocity and density profiles are:

- smooth density profile function:

$$\rho(x) = \frac{\rho_1 + \rho_2}{2} - \frac{\rho_2 - \rho_1}{2}\frac{x}{H} \tag{34}$$

- smooth velocity profile function:

$$U(x) = \frac{U_1 + U_2}{2} - \frac{U_2 - U_1}{2} tanh\left(9\frac{x}{H}\right) \tag{35}$$

In this case, we verified the Richardson number criterion (there are points in the domain where the local Richardson number is smaller than 0.25, which leads to instability in the system).

We evaluate the flow evolution for both discontinuous (Figs 1-2) and continuous case (Figs. 3-4) of the Kelvin-Helmholtz instability. The implementation of the combination WENO5-Rusanov and WENO5-HLLC was tested by performing computations for two different Cartesian meshes with spatial resolutions of 250^2 and 500^2 at different time instants $t_1 = 0{,}72s, t_1 = 1{,}02s$ and $t_1 = 1{,}38s$, respectively.

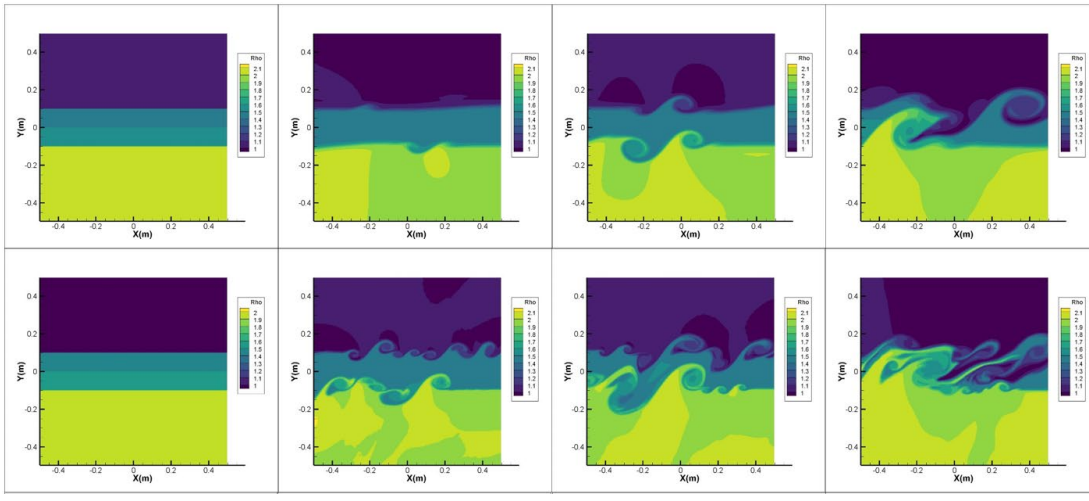

Fig. 3 The evolution of density field for the Kelvin-Helmholtz instability for continuous velocity and density profiles, 250×250 grid points, Rusanov versus HLLC solver performance
$(t_0 = 0s, t_1 = 1{,}48s, t_1 = 2{,}02s, t_1 = 3{,}28s)$

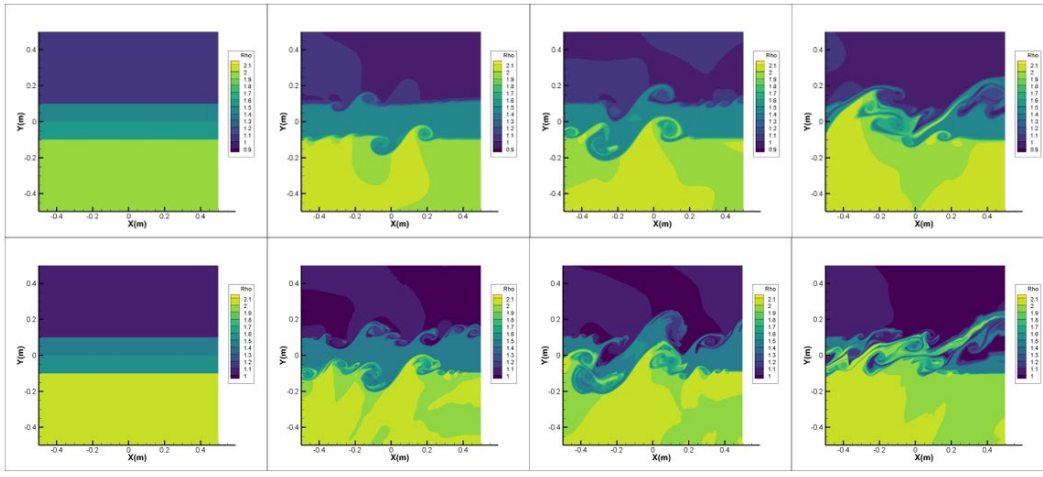

Fig. 4 The evolution of density field for the Kelvin-Helmholtz instability for continuous velocity and density profiles, $500x \times 500$ grid points, Rusanov versus HLLC solver performance
$(t_0 = 0\,s, t_1 = 1{,}48s, t_1 = 2{,}02s, t_1 = 3{,}28s)$

Looking at the results, we can find that the combination scheme WENO5-HLLC is much less dissipative at small scales and produces more numerous small vortices. The interface simulation between two fluids is quite sensitive to the dissipation of numerical method. Regarding the pattern of the flow we remark that as long as the disturbances are amplified, the arrangement of vorticity corresponds to two parallel vortex rows which are displaced relative to one another. As equilibrium state exists no more, the elementary vortices have a tendency to rotate around their centre or, to slip around each other. Due to the advected velocity, the

vortices slowly become bigger vortices with time by a vortex merging mechanism. This process have been confirmed in experiments [14].

7. CONCLUSIONS

The paper outlines the important equations which describe the flow physics, specifically to the Kelvin-Helmholtz instability and the Taylor–Goldstein equation. The numerical benchmark tests confirm the theory this paper is based on and provide a pattern of realistic density stratified shear flows in the presence of a free surface. Critical wavelength and Richardson number criterions are verified for each of the Kelvin-Helmholtz instability studied case (continuous and discontinuous, respectively). Based on the numerical results, we can also notice a better performance of the HLLC solver compared to Rusanov solver. We want to mention that we have also performed the same tests with HLL (Harten-Lax-van Leer) solver but because the results were not significantly different from those given by Rusanov we choose not to publish them. Moreover, we find that increasing the number of grid points leads to a better accuracy in shear layer vortices visualization. However, numerical tests were severely limited by the computational resources available. Further exploration of the topic includes calculations on different solvers, better grid domains, increase of the discretization methods used accuracy or extension of the study to a tridimensional case.

ACKNOWLEDGEMENT

This article is an extension of the paper presented at ***The 39th "Caius Iacob" Conference on Fluid Mechanics and its Technical Applications***, 28 – 29 October 2021, Bucharest, Romania, Virtual Conference, Section 2 – Equations of Mathematical Physics.

REFERENCES

[1] P. Hazel, Numerical studies of the stability of inviscid stratified shear flows, *J. Fluid Mech*., **51** (1), 39–61, 1972.
[2] B. Cushman-Roisin, *Environmental Fluid Mechanics*, John Wiley & Sons, 2019
[3] P. K., Kundu, I. M. Cohen, *Fluid Mechanics*, 3rd ed., Elsevier Academic Press, 759 pp., 2004.
[4] L. Gramer, *Kelvin-Helmholtz Instabilities*, GFD II, 2007.
[5] A. A. Gavrilieva, Yu. G. Gubarev, M. P. Lebedev, The Miles Theorem and the first boundary value problem for the Taylor–Goldstein equation, *J. Appl. Industr. Math*., 13:3, 460–471, 2019.
[6] E. Torro, *Riemann Solvers and Numerical Methods for Fluid Dynamic*, Springer, 2009.
[7] J. W. Miles, On the stability of heterogeneous shear flows, J. *Fluid Mech*., **10**, 496–508, 1961.
[8] P. G. Drazin and L. N. Howard, Hydrodynamic Stability of Parallel Flow of Inviscid Flow, *Advances in Applied Mechanics,* vol. **9**, 1966.
[9] C. W. Shu, High Order ENO and WENO Schemes for Computational Fluid Dynamics, *High-Order Methods for Computational Physics,* vol. **9**, 1999.
[10] P. Zhang and J. Wang, A Newly Improved WENO Scheme and its Application to the Simulation of Richtmyer-Meshkov Instability, *Procedia Engineering*, vol. **61**, 2013.
[11] G. S. Jiang and C. W. Shu, Efficient Implementation of Weighted ENO Schemes, *Journal of Computational Physics,* vol. **126**, 1996.
[12] S. Gottlieb and C. W. Shu, Total Variation Diminishing Runge-Kutta Schemes, *Mathematics of Computation,* vol. **67**, 1996.
[13] A. Harten, S. Osher, B. Engquist, S. R. Chakravarthy, Some results on uniformly high-order accurate essentially nonoscillatory schemes, *Applied Numerical Mathematics*, **2(3)**:347-377, 1986.
[14] A. Michalke, On the inviscid instability of the hyberbolic tangent velocity profile, *J. Fluid Mech*., **19**:543–556, 1964.